

Theoretical study of UHPCC composite column behaviors under axial compression

Xiang-Guo Wu^{*1,2}, Ruofei Zou^{3a}, Xinyu Zhao^{4b} and Qun Yu^{4c}

¹Key Lab of Structures Dynamic Behavior and Control, Harbin Institute of Technology, Ministry of Education, Heilongjiang, Harbin, 150090, China

²School of Civil Engineering, Harbin Institute of Technology, Heilongjiang, Harbin 150090, China

³Department of Civil and Environmental Engineering, University of Illinois, IL 61801-2352, USA

⁴School of Architecture Engineering, Harbin Engineering University, Harbin 150001, China

(Received May 7, 2013, Revised May 16, 2014, Accepted June 10, 2015)

Abstract. To improve the durability and service life of reinforced concrete column such as bridge piers, an advanced composite column made of Ultra High Performance Cementitious Composites (UHPCC) permanent form is proposed. Based on elasticity plasticity theory, axial compression behavior of the composite column was studied theoretically. The first circumferential cracking load and ultimate limit loading capacity are derived for the composite column. Short composite column compression tests and numerical simulations using FEM method were carried out to justify the theoretical formula. The effects of UHPCC tube thickness on the axial compression behavior were studied. Using the established theoretical model and numerical simulation, the large dimension composite columns are calculated and analyzed with different UHPCC tube thickness. These studies may provide a reference for advanced composite column design and application.

Keywords: ultra high performance cementitious composites; composite column; cracking load; ultimate limit loading capacity; short column compression test

1. Introduction

The construction of a gravity pier normally requires steel cyclic formwork. However, installation and dismantlement of steel cyclic formwork consumes significant work-hours. Traditional steel formwork has a high cost due to materials and haulage. Additionally, in traditional gravity pier construction, concrete surfaces are exposed to the elements immediately after de-molding. Traditional gravity pier durability properties are also lower, especially for railway bridge piers. To address structural durability deterioration due to normal concrete cracking and low durability, Maalej and Li (1995) proposed substituting the reinforced steel coat layer of normal concrete for strain hardening Engineered Cementitious Composites (ECC). Based on this

*Corresponding author, Professor, E-mail: wuxiangguo@hit.edu.cn

^aPh.D. Student, E-mail: rzou3@illinois.edu

^bPh.D. Student, E-mail: zhaoxinyu@hrbeu.edu.cn

^cEngineer, E-mail: dacong1986@126.com

design concept, a composite flexural beam with ECC coat layer was tested in their laboratory. To improve existing bridge pier service life, the Railway Transportation Management Center of China (RTMCC) also proposed the design concept of pier protection plate, which has since been applied to existing railway bridge piers to improve structural durability (MREMC of P.P.C. 2009). However, these design concepts only concentrated on improving traditional structural durability. ECC coat layer and pier protection plate cannot contribute to the composite structural strength. The more reasonable material for high durability composite structure should possess high durability and high strength. Ultra High Performance Cementitious Composite (UHPCC) is proposed here for the advanced design of high durability hybrid pier structures.

UHPCC is obtained by mixing short and thin steel fiber, a high strength cementitious matrix, and mineral admixtures with a special mixing technique and curing system. UHPCC exhibits high mechanical and durability properties with compressive strength in the range 80-400MPa, tensile strength 10-30MPa, and elastic modulus 40-50GPa. UHPCC is an advanced material with many superior performance factors. UHPCC is a new generation of engineering structural material that will replace normal strength concrete and normal high strength concrete in future designs (Wu and Xu 2009). Recently, a number of researchers have carried out extensive research and engaged in international communication in the areas of material strain hardening behavior (Wu and Han 2009), constitutive property behavior of UHPCC (Williams *et al.* 2010), strength model (Ramadoss and Nagamani 2008), UHPCC behavior under multi-axial compression (Kittinun *et al.* 2010), and interface performance of UHPCC hybrid elements (Wu and Han 2010). Some new types of structures employing UHPCC were developed recently, such as Shepherds Creek Bridge in Australia (Cavill *et al.* 2003), Wapello Bridge in Iowa, USA (Graybeal *et al.* 2004), Kuysu High Speed Bridge in Japan (Okuma 2004), FHWA short span bridge in the USA (Graybeal *et al.* 2004), and the Saint-Pierre-La-Cour hybrid bridge in France (Behloul 2007). The design of hybrid bridge decks with prefabricated UHPCC plate results in a weight reduction factor of 2.2. The application of these new hybrid structures grants benefits in cost, construction speed, structural durability, and material-saving design.

Design of hybrid pier with UHPCC permanent form is proposed by Wu *et al.* (2011). In the new type of structural member, UHPCC permanent form acts as formwork during the construction stage, and as protection plate post-construction, and also as a coat layer for the interior reinforced steel. UHPCC permanent form holds some characteristics such as high strength, high durability and light weight. Hence, this new form is named *multifunctional permanent formwork*. According to this background, a new composite column with UHPCC tube is proposed in this paper.

UHPCC composite column under axial compression are studied in this paper including the ultimate limit loading capacity, the first cracking load and ductility. Axial compression of short composite column and numerical simulations based on ABAQUS software were carried out to validate the theoretical model and formulas proposed in this paper. Comparisons of the ultimate limit loading capacities between UHPCC composite column and reinforced NC column with the same geometrical dimensions show that the loading capacity of UHPCC composite column is considerably improved. The wall thickness of UHPCC tube is proposed and finally a proposed application of UHPCC permanent form is illustrated. These studies may provide a reference or design basis for UHPCC composite column design and application in bridge pier and semi-precast assembling reinforced concrete structural system in which UHPCC precast element can be used as permanent form.

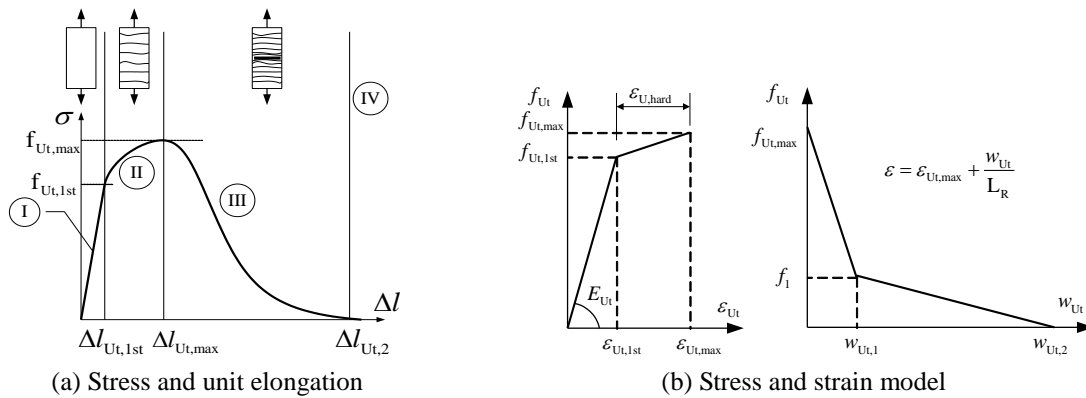


Fig. 1 Tensile model of UHPCC

Table 1 Parameters of UHPCC tensile constitutive model

$f_{Ut,1st}$	$\epsilon_{Ut,1st}$	$f_{Ut,max}$	$\epsilon_{Ut,max}$	E_{Ut}	f_1	$w_{Ut,1}$	$w_{Ut,2}$	L_R
6-8 MPa	100 $\mu\epsilon$	15 MPa	2000-4000 $\mu\epsilon$	40 GPa	2.5 MPa	2 mm	6.5 mm	270 mm

2. Basic mechanics model of the materials

2.1 Uniaxial tensile behavior of UHPCC

According to the results of the uniaxial tensile test and cylinder splitting test, the tensile strength of the UHPCC with compressive strength 120 MPa is about 6 to 15 MPa, which is dependent on fiber parameters such as steel fiber volume fraction. This tensile strength is about 3 to 8 times that of normal concrete. The tensile stress zone cannot be omitted in the UHPCC hybrid structure analysis, which is the main difference from reinforced normal concrete structure. Hence, the axial tensile performance of UHPCC is introduced first here.

As seen in the full process curve of tension stress and unit elongation, deformation of UHPCC under uniaxial tension can be divided into four parts as shown in Fig. 1(a).

The first part is the quasi linear elastic stage before the initial cracking stress. Initial micro-cracking of material exists in the UHPCC matrix in this stage. As the load increases, these initial cracks will propagate and connect with each other. With bridging of the steel fiber, the rigidness of the material is almost invariable. The second part is the strain hardening stage. In this stage, a micro-crack develops into a macro-crack and the material rigidness will be significantly decreased. With fiber reinforcement, the material is deformed with multiple cracking behaviors. The third part is the softening stage. In this stage, deformation will be localized as one single crack or several local cracks and is related to the energy dissipation capability of each macro-crack. The process of localized deformation is accompanied by fiber pulling-out and de-bonding behavior. Finally, the structural element will fail with a single main crack. The last part is the fiber pulling-out stage in which fiber pulling-out will be stopped in a localized crack. The material is in a fracture state without any stress and the structural element fails in fracture.

The uniaxial tensile hardening stress and strain relation of UHPCC is shown in Fig. 1(b) and the expression can be written as Eq. (1). The model parameters of a corresponding axial tension test are shown in Table 1.

$$f_{Ut} = \frac{E_{Ut} e}{(f_{Ut,max} - f_{Ut,1st})(e - e_{Ut,1st}) / (e_{Ut,max} - e_{Ut,1st}) + f_{Ut,1st}} \quad \begin{matrix} 0 < e? & e_{Ut,1st} \\ e_{Ut,1st} < e? & e_{Ut,max} \\ e_{Ut,max} < e? & w_{Ut,1} \\ w_{Ut,1} < e? & w_{Ut,2} \end{matrix} \quad (1)$$

2.2 Compression modulus of UHPCC

The compressive strength is limited to 120MPa for UHPCC permanent form design. According to ACI 363R (ACI Committee 363 1992), Ma (Ma et al 2004), and Benjamin (Benjamin 2005 and 2007), the modified compression modulus of UHPCC is proposed statistically as $E_{Uc} = 3840\sqrt{f_{Uc}'}$. Here, f_{Uc}' is the compressive strength of a UHPCC cylinder specimen with diameter 100mm and height 200mm. E_{Uc} is the compressive modulus of UHPCC.

2.3 Mixing compositions of UHPCC with compressive strength 120MPa

Mix compositions of UHPCC with compressive strength 120MPa are shown in Table 2. Fine silica sand is substituted by normal sand from the Songhua River to reduce the material cost. The steel fiber mixing volume fraction is 2% of the composites. Precise information of the composite material and mixing technique of UHPCC can be obtained from (Wu and Zhao 2011).

2.4 Simplified model and parameters of UHPCC for structural analysis

For simplification and conservative analysis, the strain hardening region is omitted here. The compressive strength of UHPCC is selected as 120MPa with a uniform modulus 40 GPa. This simplification agrees with the model of UHPCC proposed by FHWA Report (Benjamin 2006) as shown in Fig. 2.

Table 2 Mix compositions of UHPCC (kg/m³)

Cement	Silica fume	Filling powder	Fine sand	Super Plast.	Water	Expan. agent	Defoamer	Steel fiber
789.75	197.44	157.95	868.72	31.59	197.44	3.95	3.95	102.41

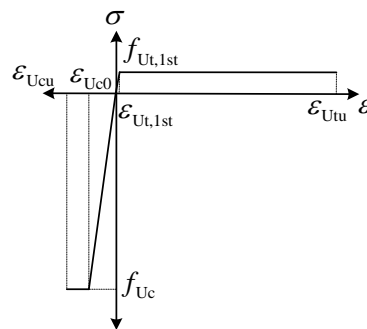


Fig. 2 Simplified tensile and compressive stress-strain model of UHPCC

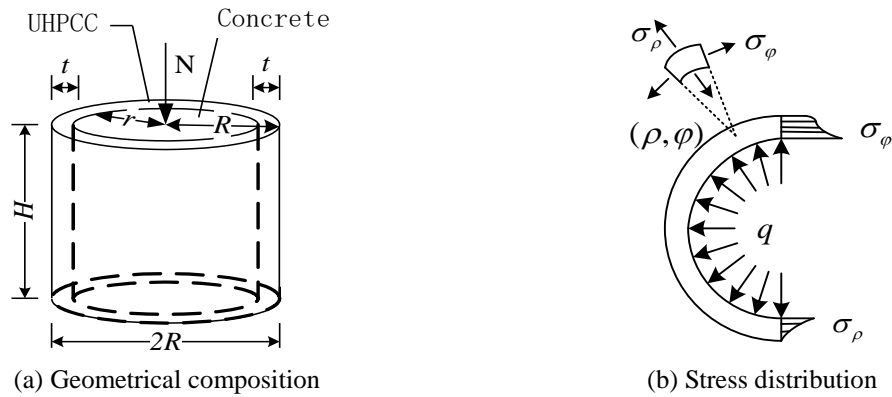


Fig. 3 UHPCC composite column and stress distribution

2.5 Normal concrete and reinforced steel

Normal Concrete (NC) with compressive strength 30MPa and Reinforced Steel (RS) of HRB335 are considered in UHPCC composite column. The ideal elastic plastic model is used for the uniaxial stress and strain relationship of reinforced steel. The uniaxial compressive stress and strain relationship of NC can be written as

$$\sigma_c = \begin{cases} f_c \left[1 - \left(1 - \frac{\varepsilon}{\varepsilon_0} \right)^n \right] & 0 < \varepsilon \leq \varepsilon_0 \\ f_c & \varepsilon_0 < \varepsilon \leq \varepsilon_{cu} \end{cases} \quad (2)$$

3. Theoretical model of axial compression for UHPCC composite column

A UHPCC composite column is composed of a UHPCC circular tube element and core reinforced NC element as shown in Fig. 3. The geometrical parameters relation can be written as $R-t=r$. In which, R is the radius of the composite column, r is the radius of the core NC element, and t is the thickness of UHPCC tube.

Each element contributes to the structural loading capacity. Because of UHPCC high tensile strength and ductile behavior, the NC is constrained circumferentially by the UHPCC tube and the core NC element is compressed in three dimensions. Thus, the core NC element loading capacity can be improved. This principle is the same as steel tube concrete structures.

The Failure processes of UHPCC composite column under axial loading can be divided into three stages: (1) quasi-elastic stage from initial loading to first cracking, (2) working with cracks from first cracking to ultimate state of core NC, and (3) failure stage from ultimate compression of core NC to yielding state of RC. To improve the composite column durability, UHPCC materials holding high durability is only one aspect. Crack development should also be limited at service stage to ensure structural durability. Therefore, the first cracking state is the key failure mode which should be controlled for high durability design of UHPCC composite column. Based on first cracking loading capacity, ultimate limit loading capacity of UHPCC composite column is also

analyzed in this paper.

3.1 The first cracking loading capacity under axial compression

According to the service practices of pier structures, the following five assumptions are considered in the analysis of loading capacity of UHPCC composite column: (1) axial load is considered a concentrated load and acts on the upper surface; (2) the influences of micro non-uniformity of UHPCC and NC on mechanics behavior are ignored; (3) radial displacements between core NC and UHPCC tube are compatible with each other and tangential stress at the interface is ignored; (4) the radial strain resulting from gravity and loading can be superposed linearly; and (5) cross section analysis of the composite column is considered as plane strain state.

A cross section with distance l which is far enough from the acting surface will be analyzed as follow. When loading, UHPCC tube is acted on with distributed stress q by the core NC element as shown in Fig. 5(b). From the Lamé solution of elasticity theory, radial stress and circumferential stress at any point (ρ, φ) of UHPCC tube can be written as

$$s_r = -\frac{\frac{R^2}{r^2} - 1}{\frac{R^2}{r^2} - 1} q, \quad s_\varphi = \frac{\frac{R^2}{r^2} + 1}{\frac{R^2}{r^2} - 1} q \quad (3)$$

In which, ρ is the radial coordinates $[r, R]$, φ is the circumferential coordinates $[0, \pi]$, σ_ρ is the radial stress at coordinate ρ , σ_φ is the circumferential stress at coordinate ρ , and q is the compressive stress from the core NC element (absolute value).

When $\rho=r$, the absolute values of σ_ρ and σ_φ are at maximum. The first cracking state of a composite column can be expressed as

$$\sigma_\varphi|_{\rho=r} = f_{U_t,1st} = \frac{\frac{R^2}{r^2} + 1}{\frac{R^2}{r^2} - 1} q \quad (4)$$

$$\sigma_\rho|_{\rho=r} = -q \quad (5)$$

Here, $f_{U_t,1st}$ is the first tensile cracking strength of UHPCC(MPa).

From Eq. (4), the radial stress q at the first cracking state of composite column can be written as

$$q = \frac{\frac{R^2}{r^2} - 1}{\frac{R^2}{r^2} + 1} f_{U_t,1st} \quad (6)$$

The corresponding circumferential strain can be written as

$$\varepsilon_\varphi = \frac{1 - \mu_U^2}{E_U} \left(\sigma_\varphi - \frac{\mu_U}{1 - \mu_U} \sigma_\rho \right) \quad (7)$$

Here, ε_ϕ is the circumferential strain at radius ρ . μ_U is the Poisson ratio of UHPCC. E_U is the elastic modulus of UHPCC.

By substituting (4), (5) and (6) into (7), Eq. (7) can be written as

$$\varepsilon_\phi \Big|_{\rho=r} = \frac{1-\mu_U^2}{E_U} \left(f_{Ut,1st} + \frac{\mu_U}{1-\mu_U} \cdot \frac{\frac{R^2}{r^2}-1}{\frac{R^2}{r^2}+1} f_{Ut,1st} \right) \quad (8)$$

According to the geometrical relation of plane axial symmetrical problem of elasticity theory, the relation between radial displacement and circumferential strain can be expressed as

$$u_\rho = \rho \varepsilon_\phi \quad (9)$$

Here, u_ρ is the radial displacement at radius ρ .

By substituting (8) into (9), the radial displacement of point $\rho=r$ at the interface of the UHPCC tube can be obtained as

$$u_\rho \Big|_{\rho=r} = r \cdot \frac{1-\mu_U^2}{E_U} \left(f_{Ut,1st} + \frac{\mu_U}{1-\mu_U} \cdot \frac{\frac{R^2}{r^2}-1}{\frac{R^2}{r^2}+1} f_{Ut,1st} \right) \quad (10)$$

Based on Assumption (4), the radial displacement of the core NC element is also equal to $u_\rho \Big|_{\rho=r}$. Then, concrete Poisson ratio can be expressed as

$$\mu_c = \left| \frac{\varepsilon_c'}{\varepsilon_c} \right| \quad (11)$$

Here, ε_c' is the lateral linear strain of core NC, ε_c is the longitudinal linear strain of the core NC element, and μ_c is the Poisson ratio of the NC core.

The lateral linear strain of the core NC element can be simplified as

$$\varepsilon_c' = \frac{u_\rho \Big|_{\rho=r}}{r} \quad (12)$$

By substituting (12) into (11), the expression can be written as

$$\varepsilon_c = \frac{u_\rho \Big|_{\rho=r}}{r \mu_c} = \frac{1-\mu_U^2}{\mu_c E_U} \left(f_{Ut,1st} + \frac{\mu_U}{1-\mu_U} \cdot \frac{\frac{R^2}{r^2}-1}{\frac{R^2}{r^2}+1} f_{Ut,1st} \right) \quad (13)$$

Since the thickness of UHPCC tube is relatively small, deformation conditions can be assumed as

$$\varepsilon_s = \varepsilon_U = \varepsilon_c \tag{14}$$

With physical relation

$$\sigma'_s = \begin{cases} E_s \varepsilon & \varepsilon \leq \varepsilon_y = \frac{f_y}{E_s} \\ f_y & \varepsilon > \varepsilon_y \end{cases} \tag{15}$$

Here, constitution relation of the NC core can be simplified as

$$\sigma_c = \begin{cases} \frac{f_c}{\varepsilon_0} \varepsilon_c & 0 \leq \varepsilon_c \leq \varepsilon_0 \\ f_c & \varepsilon_c > \varepsilon_0 \end{cases} \tag{16}$$

And the constitution relation of UHPCC can be written as

$$\sigma_{Uc} = \begin{cases} E_U \varepsilon & 0 < \varepsilon \leq \varepsilon_{Uc0} \\ f_{Uc} & \varepsilon_{Uc0} < \varepsilon \leq \varepsilon_U \end{cases} \tag{17}$$

Based on the equilibrium condition

$$N = \sigma_c A_c + \sigma_s A_s + \sigma_U A_U \tag{18}$$

and according to three dimension compression results from the NC cylinder, the three stresses conform to

$$\sigma_1 = \sigma_{c\perp} + 4\sigma_2 \tag{19}$$

In which, $\sigma_{c\perp}$ is the stress of NC under uni-axial compression.

$$\sigma_{c\perp} = E_c \varepsilon_c \tag{20}$$

The stirrups are proposed to be remained with the consideration of longitudinal bar fixing and avoiding local imperfection of UHPCC resulted from fiber distribution. But the reinforcement ratio of the stirrup can be reduced to be minimum value of the stirrup ratio according the reinforced concrete code. Considering the structure reinforced by a stirrup, the stress distribution of the region between stirrups with height S is analyzed here as shown in Fig. 4.

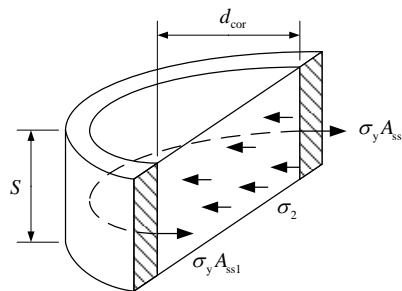


Fig. 4 Lateral stress distribution

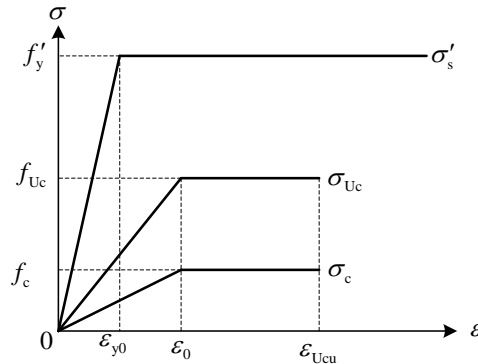


Fig. 5 Simplified compressive stress-strain relation of the materials

The equilibrium relation of the section can be written as

$$\sigma_2 S d_{cor} = 2\sigma_y A_{ss1} + 2\sigma_{Ut} St_U \tag{21}$$

In which, A_{ss1} is the cross section area of the stirrup wire, S is the distance between stirrup wires, d_{cor} is the diameter of the stirrup hoop, σ_{Ut} is the circumferential tensile stress of the UHPCC element, t_U is the thickness of the UHPCC element, and σ_y is the stirrup stress.

Expression (21) can be written as

$$\sigma_2 = \frac{2\sigma_y A_{ss1}}{S d_{cor}} + \frac{2\sigma_{Ut} St_U}{S d_{cor}} \tag{22}$$

Substituting (22) into (19)

$$\sigma_1 = \sigma_{c\perp} + \frac{8\sigma_y A_{ss1}}{S d_{cor}} + \frac{8\sigma_{Ut} St_U}{S d_{cor}} \tag{23}$$

And then

$$\begin{aligned} N_u &= \sigma_1 A_c + \sigma'_s A'_s + \sigma_{Uc} A_U \\ &= \sigma_{c\perp} A_c + \frac{8\sigma_y A_{ss1} A_c}{S d_{cor}} + \frac{8\sigma_{Ut} St_U A_c}{S d_{cor}} + \sigma'_s A'_s + \sigma_{Uc} A_U \end{aligned} \tag{24}$$

Here, stress components σ_y , σ_{Ut} , σ'_s and σ_{Uc} are unknowable and these unknowable components will be determined according to analysis at different stages. Compressive stress-strain relations of reinforced steel, NC core, and UHPCC are simplified as shown in Fig. 5.

When UHPCC cracking occurs, Eqs. (8) and (13) can be obtained. Then the stirrup stress at interface of the UHPCC element can be written as

$$\sigma_y = E_s \varepsilon_\varphi \Big|_{\rho=r} \tag{25}$$

$$\sigma_{Ut} = f_{Ut,1st} \tag{26}$$

$$\sigma'_s = E_s \varepsilon_c \quad (27)$$

$$\sigma_{Uc} = E_{Uc} \varepsilon_c \quad (28)$$

Derivation of (13) is based on the first cracking condition of UHPCC in which the hoop of UHPCC element on the core NC element is already considered, i.e., the effects of the UHPCC tube on the core NC is already included in the expression ε_c . The effects of UHPCC on the core NC element are not considered again in solving for the loading capacity of the core NC element. But effects of the stirrup should be considered. Therefore, the item $\frac{2\sigma_{Uc}St_U}{Sd_{cor}}$ in expression (22) can be omitted and expression (22) can be rewritten as

$$\sigma_2 = \frac{2\sigma_y A_{ss1}}{Sd_{cor}} \quad (29)$$

For different ε_c , (24) can be written as

$$N_u = \begin{cases} \sigma_{c\perp} A_c + \frac{8E_s \varepsilon_\phi \big|_{\rho=r} A_{ss1} A_c}{Sd_{cor}} + E_y \varepsilon_c A'_s + E_{Uc} \varepsilon_c A_U & \varepsilon_c < \varepsilon_{y0} \\ \sigma_{c\perp} A_c + \frac{8E_s \varepsilon_\phi \big|_{\rho=r} A_{ss1} A_c}{Sd_{cor}} + f_y A'_s + E_{Uc} \varepsilon_c A_U & \varepsilon_{y0} \leq \varepsilon_c < \varepsilon_0 \\ \sigma_c A_c + \frac{8E_s \varepsilon_\phi \big|_{\rho=r} A_{ss1} A_c}{Sd_{cor}} + f_y A'_s + f_{Uc} A_U & \varepsilon_0 \leq \varepsilon_c < \varepsilon_{Ucu} \end{cases} \quad (30)$$

Formula (30) is the first cracking load of the composite column of UHPCC tube and core NC element.

3.2 Ultimate limit loading capacity under axial compression

For appropriate reinforcement design of the cross section, the ultimate state of the composite column can be defined as the state with the characteristics of yielding of longitudinal and stirrup bars, full cracking of UHPCC ($\sigma_{Uc}=0$), and compressive failure of the core NC element. Then the ultimate limit loading capacity of the UHPCC composite column can be obtained by superposition of each composition contribution.

$$N_u = f_c A_c + \frac{8f_y A_{ss1} A_c}{Sd_{cor}} + f'_y A'_s + f_{Uc} A_U \quad (31)$$

4. Test and evaluation of the composite conlumn

4.1 Axial compression test

4.1.1 Material properties

The design compressive strength of UHPCC used in the composite columns is 100~140 MPa.

Fine aggregate selection breaks through the limitation of traditional UHPCC on quartz sand. The domestic washing river sand with size 0.5 mm below is used for the fine aggregate, and its apparent density is 2.62 g/cm^3 , the content of SiO_2 is 93%. The polycarboxylate superplasticizer density is 1.01 g/cm^3 , with 30% solid content. The fineness modulus of 400 objective quartz powder is used as filler. Steel fiber volume content is 2%. The density of steel fiber is 7.5 g/cm^2 , length 15 mm, diameter 0.2 mm, and tensile strength 1400 MPa. The mixing Mix design is shown in Table 2. Specific performance of the raw material and mixing process can be referenced from the relevant literature, such as the Wu and Han (2010), Wu *et al.* (2008), Graybeal *et al.* (2004), Benjamin (2006), Wu *et al.* (2011).

4.1.2 Specimen dimension

UHPCC tubes with design compressive strength of 120 MPa were made in the structure laboratory of Harbin Institute of Technology. After molding and curing of the UHPCC pipes, normal concrete with design compressive strength of 30 MPa is filled in it. In order to study the influence of UHPCC pipe wall thickness on the mechanical properties of the composite column, here unreinforced concrete is designed. In order to study the composite effect, a hollow UHPCC tube is made. All the specimens of the number and geometry parameters are shown in Table 3 in which A_u and A_c are the cross area of the UHPCC tube and core concrete area, respectively.

4.1.3 Loading test of short composite column

In order to improve the end bearing capacity of the short column, the ends are constrained using three layers of FRP, and the end bearing surfaces are leveled using high-strength gypsum. LVDT was used to collect the axial deformation. The UHPCC composite short column specimens are loading statically using 200 tons hydraulic testing machine with continuous loading scheme and the loading rate of 0.1 ton/s. The first cracking load is recorded in the process of test. Test is ended at the unloading value of 80% of the corresponding ultimate load. As an example, the test images of the specimen SHC400-96-32 are shown in Fig. 6.

Table 3 Specimen dimension

Specimen	H (mm)	R_o (mm)	t (mm)	A_u ($\times 10^3 \text{ mm}^2$)	A_c ($\times 10^3 \text{ mm}^2$)
SHC400-96-15	400	96	15	8.33	20.60
SHC400-96-32	400	96	32	16.07	12.86
SHC400-96-42	400	96	42	19.78	9.15
HHC400-96-32	400	96	32	16.07	12.86



Fig. 6 Specimen loading and failure state

Table 4 Axial compression test results

Specimen	Ultimate load ($\times 10^3$ kN)			Cracking load ($\times 10^3$ kN)			Cracking disp. (mm)	G_c (kN•mm)	G_{3c} (kN•mm)	I_5
	<i>N</i>	<i>T</i>	<i>M</i>	<i>N</i>	<i>T</i>	<i>M</i>				
SHC400-96-15	1.90	1.71	1.45	0.85	0.90	0.47	0.241	109.40	978.56	8.94
SHC400-96-32	2.68	2.64	1.99	1.01	1.20	0.63	0.262	144.66	1355.02	9.37
SHC400-96-42	3.03	3.2	2.25	1.08	1.20	0.73	0.210	134.13	766.82	5.72
HHC400-96-32	2.17	1.82	—	0.72	0.62	—	0.1765	57.36	474.88	8.28

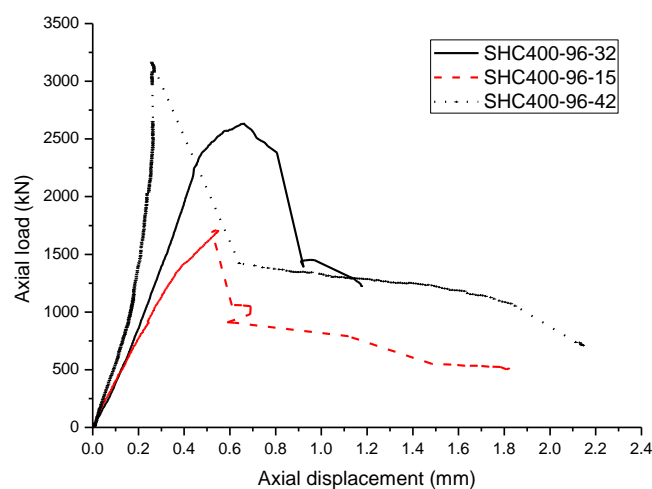


Fig. 7 The load displacement curves of the composite column

4.2 Test results analysis

4.2.1 Test results

Axial compression test results are shown in Table 4, including the ultimate bearing capacity, cracking load and crack displacement. In the table, '*N*', '*T*' and '*M*' represent numerical simulation result, test result and theoretical model prediction, respectively.

4.2.2 Effect of UHPCC tube thickness on axial compression strength

The load displacement curves of the composite column specimen with different UHPCC tube wall thickness are shown in Fig. 7. As can be seen from the figure, when the UHPCC tube wall thickness are 15 mm, 32 mm and 42 mm, axial compressive ultimate strength are respectively 1710 kN, 2640 kN and 3200 kN, and the first cracking load are 900 kN, 1200 kN and 1200 kN, respectively. In addition, ductility of the axial compression column increases firstly, then decreases. Wall thickness of the corresponding best ductility is 32 mm which is mainly caused by the size effect of the tensile properties of UHPCC materials. This comparison shows the effects of thickness on the ductility. This test concentrated on the SHC specimen without transverse bar which should be considered in engineering, but its ratio can be reduced significantly due to fiber reinforcement contribution. Therefore, the benefit of using UHPCC composite column can increase the ductility with reduced the transverse bar ratio.

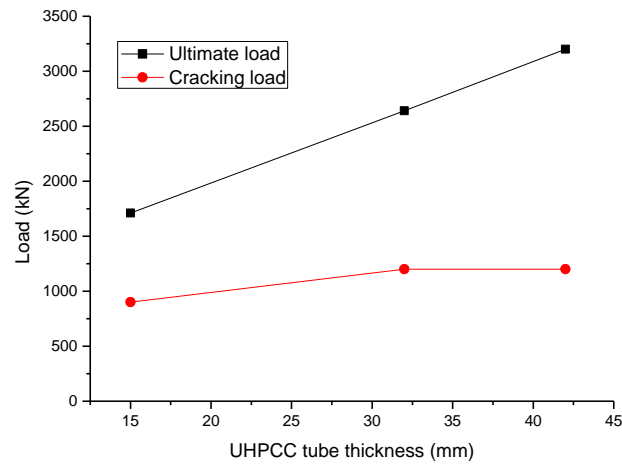
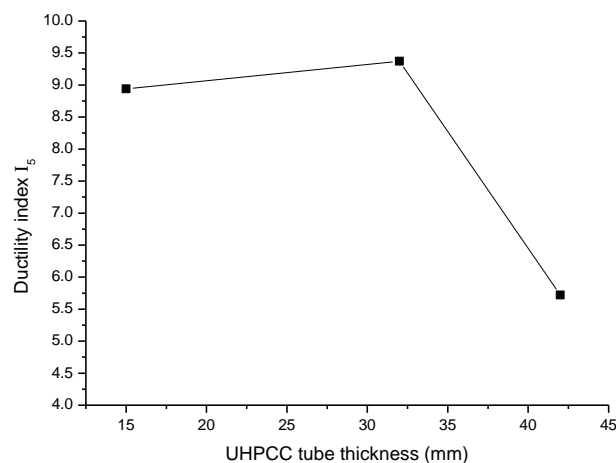


Fig. 8 Strength variation with UHPCC tube wall thickness

Fig. 9 Effect of UHPCC pipe thickness on ductility index I_5

The variation of the initial crack load and ultimate limit load with UHPCC wall thickness are shown in Fig. 8. As can be seen from the figure, along with the UHPCC pipe wall thickness increasing, the ultimate bearing capacity of axial compression increases linearly. While the first crack load change is different and show slow increasing trend when the wall thickness is small, but for the two cases with the wall thickness of 32 mm and 42 mm, the initial cracking load is almost unchanged. This is caused by the size effect on tensile properties of UHPCC materials. The first cracking load mainly depends on the UHPCC cracking strength and fiber distribution has an important effect on the material initial cracking strength. UHPCC wall thickness has an important influence on the distribution of fiber. This is the size effect of UHPCC material tensile property.

4.2.3 Effect of the UHPCC tube thickness on its ductility

To characterize the toughness of fiber reinforced concrete ACI Committee 544 recommends the use of ASTM C-1018 toughness measurements in bending. The toughness I_5 index represents the

area under the load deflection curve up to a given deflection divided by the area under the curve up to the deflection at cracking (Vellore *et al.* 1995, Balendran *et al.* 2002). The numerator of the index can be considered the total energy up to a given deflection and the denominator can be considered the elastic energy. The concept of toughness index can be extended not only to bending but also to tension, compression and shear (Naaman and Reinhardt 1995). The toughness index gives a measure of relative ductility.

The toughness index I_5 is used here to analyze the influence of UHPCC pipe wall thickness on axial compression ductility. The energy consumption G_c corresponding to the first cracking state and the total energy consumption G_{3c} corresponding to the 3 times the initial cracking displacement, as well as the ductility index of I_5 are listed in table 4. Ductility index I_5 variations with UHPCC tube wall thickness are shown in Fig. 9.

It can be seen from the figure that the ductility is better when the UHPCC pipe wall thickness is small. The ductility of the composite column with wall thickness 32mm is better than the that with wall thickness of 15mm, but the ductility of the composite column with wall thickness of 42mm is significantly lower than that with wall thickness of 32mm. This is mainly caused by the size effect of the tensile properties of UHPCC materials. For the ideal plastic material, I_5 is equal to 5 (Naaman and Reinhardt 1995). According to the axial compressive behavior, C30 concrete is quasi brittle materials and its value of I_5 range 1~5. Thus, the ductility of UHPCC tube composite column is improved obviously compared with core concrete.

4.2.4 Comparison between composite column and hollow column

The load displacement curves of the specimen SHC400-96-32 and hollow UHPCC tube HHC400-96-32 are shown in Fig. 10. Compared with the hollow UHPCC tube, the initial cracking load is increased from 620 kN to 1200 kN, initial cracking displacement is increased from 0.1762 mm to 0.262 mm, and the axial compressive ultimate strength is increased from 1820 kN to 2640 kN.

4.3 Comparisons between test results, theoretical and numerical predictions

Using FEM software ABAQUS, the composite column of the test specimens are simulated.

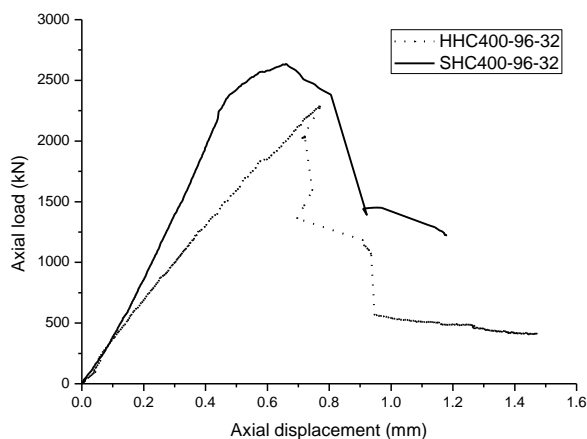
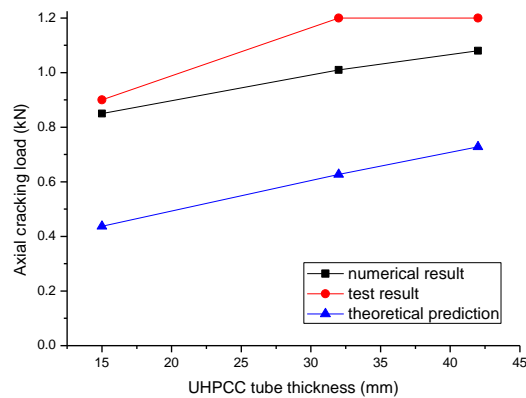


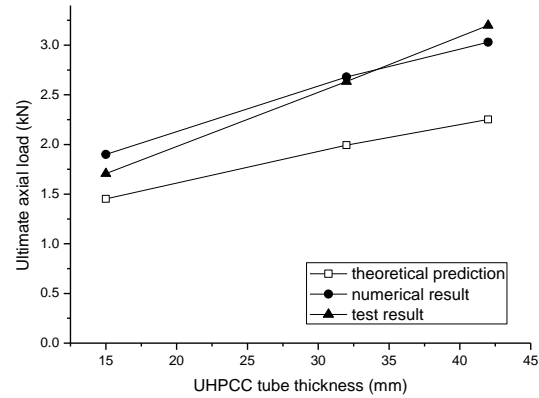
Fig. 10 Comparison between composite column and hollow UHPCC tube

Table 5 Material parameters

Material	Poison ratio	E (Pa)	Ultimate comp. strain	Comp. strength (MPa)	Cracking strain	Cracking stress (MPa)	Ultimate tensile strain
UHPCC	0.18	50e9	0.0036	100	0.00012	6	0.01
NC	0.2	15e9	0.0043	30	0.00012	1.8	0.00014
Steel bar	0.3	200e9					0.01



(a) The first cracking load



(b) Axial compressive ultimate load

Fig. 11 Results comparison of test, numerical simulation and theoretical model

Smearred cracking models are selected for UHPCC and NC. Material parameters for the simulation are listed in Table 5. Element C3D8R is selected for the simulation.

One end of the structure is given fixed boundary conditions and the other end is subjected to a concentrated load. The UHPCC tube is divided into one layer elements when tube thickness is less than 20mm. The UHPCC tube is divided into two layer elements when tube thickness equals 20mm. Numerical simulation results and the calculated results according to the theoretical model are shown in figure 11 including the first cracking load and ultimate bearing capacity.

It can be seen from the figure that the test result of the ultimate axial compression load is 1.3 times of the theoretical result and test result of the cracking load is 1.8 times of the theoretical result. The differences between the theoretical prediction and test results which may be resulted by the size effect of material properties, size effect of short column and some assumptions in the theoretical model. Numerical simulation results are good agreement with the test results. However, in the numerical model and theoretical model, the size effect caused by the three-dimensional distribution of fiber is not considered in the tensile model of materials. Hence the theoretical model cannot predict the size effect of the cracking load which is the main difference compared with the test results.

5. Axial compression behavior of large dimension component

The large dimension composite column with length 10m, diameter 1.5 m and UHPCC tube thicknesses 20 mm, 30 mm, 40 mm, 50 mm, 100 mm, 150 mm and 200 mm are simulated using the FEM software ABAQUS to compare it with the theoretical results. Material parameters for the

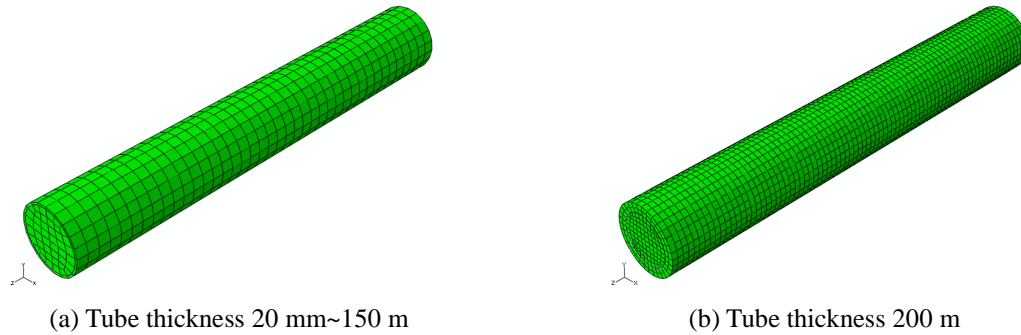


Fig. 12 Element divisions

simulation are listed in Table 6. Element division is shown in Fig. 12.

Numerical results of the composite column with typical UHPCC tube thickness 50 mm is shown in Fig. 13, which include load and axial displacement curve, load and axial strain curve, strain contour figure in x direction, stress contour figure in y direction, stress contour figure in z direction, and the axial displacement contour figure. The first cracking load and ultimate loading capacity of typical UHPCC composite column with tube thickness 20 mm, 30 mm, 40 mm, 50 mm, 100 mm, 150 mm and 200 mm were obtained and are listed in Table 7.

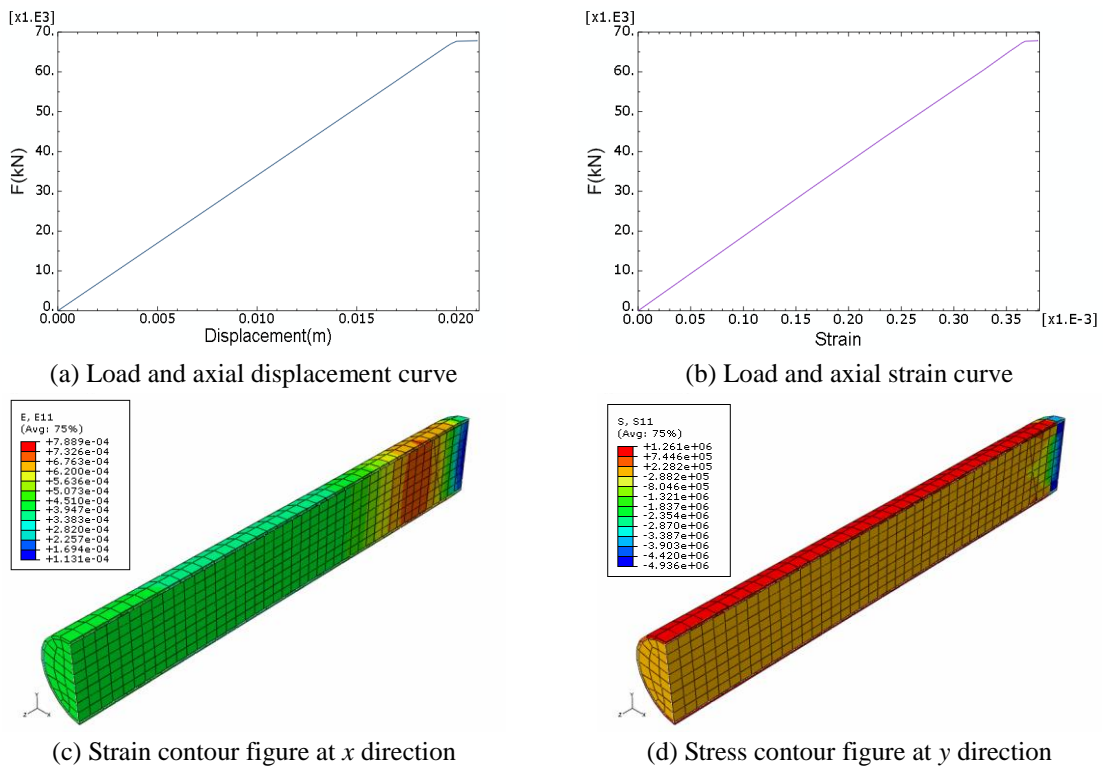


Fig. 13 Numerical results of composite column with UHPCC tube thickness 50 mm

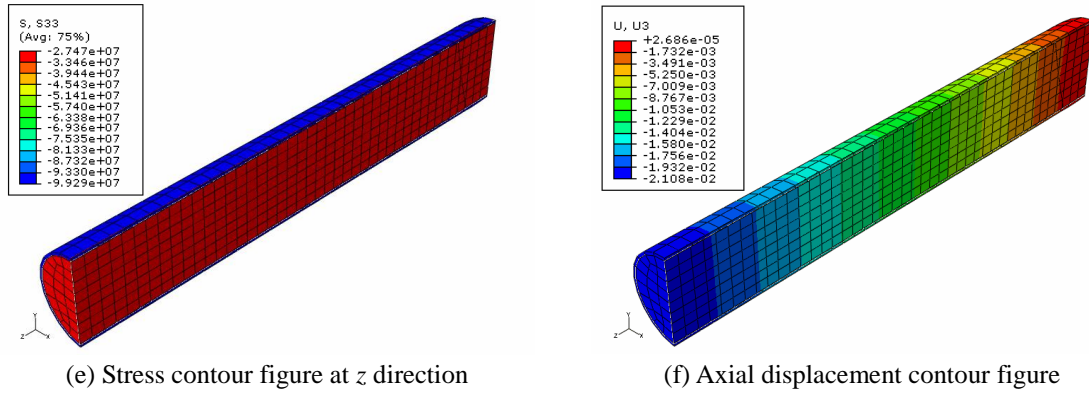


Fig. 13 Continued

Table 6 Results of theoretical and numerical

t (mm)	Cracking loading capacity			Ultimate limit loading capacity		
	M (kN)	N (kN)	D (%)	M (kN)	N (kN)	D (%)
20	17372	19302	10.00	59494	58510	1.68
30	18358	20413	10.07	62681	61629	1.71
40	19337	21446	9.83	65823	64825	1.54
50	20309	22450	9.53	68923	67690	1.82
100	25072	25392	1.26	83760	82170	1.94
150	29665	27628	-7.37	97497	95946	1.62
200	34079	34963	2.53	110136	108350	1.65

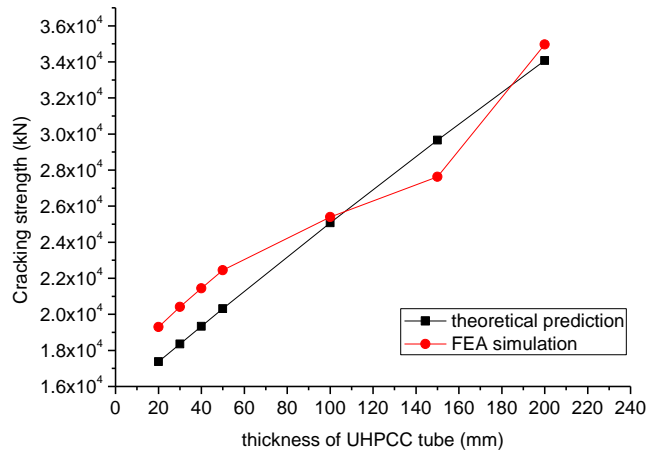


Fig. 14 Comparisons of the first cracking loading capacity results

With the typical UHPCC composite column parameters, theoretical predictions based on formulas (35) and (36) can be calculated. Theoretical model results and numerical results are all listed in Table 6, including the first cracking load and ultimate load.

Here, ' t ' is the UHPCC tube thickness. ' M ' and ' N ' represent theoretical model prediction and

numerical simulation results, respectively. ‘*D*’ means difference between theoretical and numerical results.

Comparisons between theoretical results and numerical results are drawn in Figs. 14 and 15 for the first cracking loading capacity and ultimate limit loading capacity, respectively.

It can be seen from Fig. 14 that the results based on theoretical formula proposed in this paper generally agree well with the numerical simulations. For the first cracking loading capacity, the differences are 9.53% and 7.37% for UHPCC tube with thickness less than 50 mm and equal to 150mm. When UHPCC tube thickness is 100 mm and 200 mm, the theoretical results agree well with the numerical simulations with differences of only 1.26% and 2.53%, respectively. The differences result from the elements selection, since cracks in each UHPCC FEM element may not occur simultaneously. Some elements at the maximum circumferential stress zone may fracture first and arrive at an idealized plasticity deformation region. Other elements will fracture one after another. This is multiple cracking behavior of UHPCC.

It can be seen from Fig. 15 that the results of the theoretical formula proposed in this paper for the ultimate limit loading capacity agree very well with the numerical simulations. The average difference is only 1.7%.

The ultimate limit loading capacity of the composite column with the same length and cross section made by reinforced NC material was also calculated and the results are listed in Table 8.

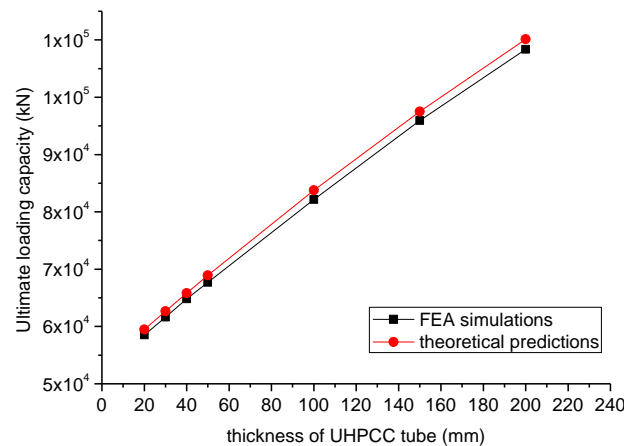


Fig. 15 Comparisons of the ultimate limit loading capacity results

Table 8 Comparisons between UCC and NCC

<i>t</i> (mm)	Ultimate limit loading capacity (kN)		Improving percentage (%)
	UCC	RCC	
20	58510	52413	11.63
30	61629	52413	17.58
40	64825	52413	23.68
50	67690	52413	29.15
100	82170	52413	56.77
150	95946	52413	83.06
250	108350	52413	106.72

Here, 'UCC' means UHPCC composite column and 'NCC' means RC column. For the minimal tube thickness of 20 mm, the improving percentage of UCC compared to NCC is 11.63%. When UHPCC tube is 50 mm, the ultimate loading capacity is improved to about 29.15% compared to traditional designs.

6. Conclusions

(1) The theoretical formula to predict the cracking load and ultimate limit loading capacity of UHPCC composite column are proposed in this paper. Theoretical predictions agree very well with nonlinear numerical simulation results for large dimension composite column. For short column, the theoretical formula predicts its cracking load and ultimate load conservatively. Comparing with the cracking load, the ultimate load predictions based on the theoretical formula are more close to the test and numerical results.

(2) UHPCC tube thickness has significant influence on the cracking load and ultimate load of the composite column. The size effect of UHPCC tube thickness on the cracking load is obvious according to the test results. UHPCC thickness 32 mm is a turning point for cracking load. Therefore, it is not better that the thickness of UHPCC tube is bigger.

(3) Compared with normal concrete column, the ductility of UHPCC composite column is improved obviously. Ductility of UHPCC composite column based on I_5 index also has size effect from UHPCC tube thickness. The composite column with UHPCC tube thickness 32 mm get the best ductile behavior.

(4) Comparisons of the ultimate limit loading capacities between large dimension composite column and reinforced NC column with the same geometrical dimensions show that the loading capacity of the composite column was improved from 11.63% to 106.27% for different tube thicknesses. The UHPCC tube minimum thickness is proposed finally no less than 20 mm, which takes into consideration the coat layer requirement for the inside reinforced bar coat layer, but no more than 40 mm which takes into consideration of the size effect on cracking load and ductility.

Acknowledgements

The authors would like to thank the National Natural Science Foundation of China (51008088), the Fundamental Research Funds for the Central Universities (Grant No. HIT. NSRIF. 2013112), Harbin City Science and Technology Innovation Talents Special Funds (2011RFLXG014), and Heilongjiang Province Natural Science Fund (E200911) (E2015014) for providing funding to this project, the National Key Technology Research and Development Program of China under Grant No. 2011BAJ10B0102, and the Scientific Technical Plan of The Ministry of Housing and Urban-Rural Development of China (2010-K2-23) for the supporting the authors' work described herein.

References

ACI Committee 363 (1992), Report on High-strength concrete (ACI 363R-92), American Concrete Institute, Farmington Hills, Mich., 55.

- Balendran, R.V., Zhou, F.P., Nadeem, A. and Leung, A.Y.T. (2002), "Influence of steel fibres on strength and ductility of normal and lightweight high strength concrete", *Build. Environ.*, **37**, 1361-1367.
- Behloul, M. (2007), "HPFRCC field of applications: Ductal recent experience", *5th High Performance Fiber Reinforced Cement Composite (HPFRCC5)*, Mainz, Germany, July.
- Benjamin, A.G. (2005), "Characterization of the behavior of ultra-high performance concrete", Doctor Thesis, University of Maryland.
- Benjamin, A.G. (2007), "Compressive behavior of ultra-high-performance fiber-reinforced concrete", *ACI Mater. J.*, **104**(2), 146-152.
- Cavill, B. and Chirgwin, G. (2003), "The world's first Ductal road bridge Sherpherds gully creek bridge, NSW", *21st Biennial Conference of the Concrete Institute of Australia*, Brisbane.
- Gopalaratnam, V.S. and Gettu, R. (1995), "On the characterization of flexural toughness in fiber reinforced concrete", *Cement Concrete Compos.*, **17**, 239-254.
- Graybeal, B.A. (2006), Structural Behavior of Ultra-High Performance Concrete Prestressed I-Girders [R], FHWA-HRT-06-115, Federal Highway Administration, New Jersey Ave., Washington.
- Graybeal, B., Hartmann, J. and Perry, V. (2004), "Ultra-high performance concrete for highway bridge", *FIB Symposium*, Avignon, April.
- Kittinun, S., Sherif, E.T. and Gustavo, P.M. (2010), "Behavior of high performance fiber reinforced cement composite under multi-axial compressive loading", *Cement Concrete Compos.*, **32**, 62-72.
- Ma, J., Dehn, F., Tue, N.V., Orgass, M. and Schmidt, D. (2004), "Comparative investigations on ultra-high performance concrete with and without coarse aggregates", *Proceedings of the International Symposium on Ultra-High Performance Concrete*, Kassel, Germany, September.
- Maalej, M. and Li, V.C. (1995), "Introduction of strain hardening engineered cementitious composites in design of reinforced concrete flexural members for improved durability", *ACI Struct. J.*, **92**(2), 167-176.
- MREMC of PPC (Engineering Management Center of The Ministry of Railways of P.P.C.) (2009), *Constructurn Manual For Reactive Powder Concrete Member*, China Railway Publishing House, Beijing. (In Chinese)
- Naaman, A.E. and Reinhardt, H.W. (1995), "Characterization of high performance fiber reinforced cement composites-HPFRCC", *Proceedings of the Second International Workshop 'High Performance Fiber Reinforced Cement Composites' (HPFRCC2)*, Ann Arbor, USA.
- Okuma, H.A., Nishikawa, K., Iwasaki, I. and Morita, T. (2006), "The first highway bridge applying ultra high strength fiber reinforced concrete in Japan", *7th International Conference on short and medium span bridge*, Montreal, Canada.
- Ramadoss, P. and Nagamani, K. (2008), "A new strength model for the high-performance fiber reinforced concrete", *Comput. Concrete*, **5**(1), 21-36.
- Williams, E.M., Graham, S.S., Akers, S.A., Reed, P.A. and Rushing, T.S. (2010), "Constitutive property behavior of an ultra-high-performance concrete with and without steel fibers", *Comput. Concrete*, **7**(2), 191-202.
- Wu, X., Han, S. and Xu, S. (2008), "Pseudo strain hardening model of ultra high performance cementitious composites under flexural loading", *Acta Materiae Compositae Sinica*, **25**(2), 129-134.
- Wu, X. and Han, S. (2010), "Interface shear connection analysis of ultra high performance fiber reinforced concrete composite girders", *J. Bridge Eng.*, ASCE, **15**(5), 493-502.
- Wu, X.G., Jiang, X.D. and Zhao, X.Y. etc. (2011), *Multiple functional permanent form for bridge gravity pier*, China Patent, Publication Number: CN 201952733 U, Open day: Aug. 31, 2011.
- Wu, X.G., Xu, S.L. and Wu, M.X. (2009), "Fracture parameters study and application of ultra high performance fiber reinforcement concrete", *Eng. Mech.*, **26**(3), 93-98.
- Wu, X.G., Zhao, X.Y. and Han, S.M. (2011), "Structural analysis of circular UHPCC form for hybrid pier under construction loads", *Steel Compos. Struct.*, **12**(2), 167-180.

Notations

- R , r and t : radius of composite column, radius of core NC element and thickness of UHPCC tube
 ρ and φ : radial coordinates [r , R] and circumferential coordinates [0 , π]
 σ_ρ and σ_φ : radial stress and circumferential stress at coordinate ρ , respectively
 q : compressive stress from core NC element (absolute value)
 A_{ssl} : cross section area of stirrup wire
 S : distance of stirrup wire
 d_{cor} : diameter of stirrup hoop
 σ_{Ut} : circumferential tensile stress of UHPCC element
 t_U : thickness of UHPCC element
 σ_y : stirrup stress
 f_{Uc}' : compressive strength of UHPCC cylinder specimen with diameter 100 mm and height 200 mm
 E_{Uc} : is compressive modulus of UHPCC
 f_y : yielding stress of reinforced bar
 ε_y : yielding strain of reinforced bar
 ε_{su} : ultimate tensile strain of reinforced bar
 f_c : ultimate compressive strength of normal concrete
 ε_0 : critical compressive strain
 ε_{cu} : ultimate compressive strain of normal concrete
 f_t : ultimate tensile strength of normal concrete
 ε_{tu} : ultimate tensile strain of normal concrete
 f_{Ut} : ultimate tensile strength of UHPCC
 $\varepsilon_{Ut,1st}$: initial tensile cracking strain of UHPCC
 ε_{Utu} : ultimate tensile strain of UHPCC
 ε_{Uc} : ultimate compressive strain of UHPCC
 f_{Uc} : ultimate compressive strength of UHPCC